The Astronomical Journal, 169:13 (16pp), 2025 January https://doi.org/10.3847/1538-3881/ad8ebe

The 10 pc Neighborhood of Habitable Zone Exoplanetary Systems: Threat Assessment from Stellar Encounters and Supernovae

Tisyagupta Pyne[1,2], Ravinder K. Banyal[1], C. Swastik[1,3,4], and Ayanabha De[1]
[1] Indian Institute of Astrophysics, Koramangala 2nd Block, Bangalore 560034, India; banyal@iiap.res.in
[2] Integrated Science Education and Research Centre, Visva-Bharati University, Santiniketan, 731235, India
[3] Dipartimento di Fisica, Università degli Studi di Milano, Via Celoria 16, 20133 Milano, Italy
[4] Pondicherry University, R.V. Nagar, Kalapet, 605014, Puducherry, India
Received 2024 August 8; revised 2024 October 27; accepted 2024 October 29; published 2024 December 9

Abstract

The habitability of a planet is influenced by both its parent star and the properties of its local stellar neighborhood. Potential threats to habitability from the local stellar environment mainly arise from two factors: cataclysmic events such as powerful stellar explosions and orbital perturbations induced by close stellar encounters. Among the 4500+ exoplanet-hosting stars, about 140+ are known to host planets in their habitable zones (HZs). In this study, we use Gaia Data Release 3 data to investigate the 10 pc stellar neighborhood of the 84 habitable zone systems (HZSs) closest to the Sun. We assess the possible risks that the local stellar environments of these HZSs pose to their habitability. In particular, we find that HD 165155 has a high stellar density around it, making it likely to experience at least one flyby encounter within a span of 5 Gyr. We also identified two high-mass stars ($M \geqslant 8\,M_{\odot}$) as potential progenitors of supernovae, which could threaten the long-term survivability of HZSs HD 48265 and TOI-1227. Further, to quantify the similarity between HZ stars and the Sun, as well as their respective 10 pc stellar environments, we employ various astrophysical parameters to define a solar similarity index and a neighborhood similarity index. Our analysis suggests that HD 40307 exhibits the closest resemblance to the solar system, while HD 165155 shows the least resemblance.

Unified Astronomy Thesaurus concepts: Solar neighborhood (1509); Exoplanet astronomy (486); Habitable zone (696); Habitable planets (695); Gaia (2360); Close encounters (255)

Materials only available in the online version of record: machine-readable table

1. Introduction

Finding a habitable world is one of the primary goals of exoplanetary research. The study of habitability is a rapidly growing field in exoplanet science, with over 150 confirmed discoveries of planets residing in the habitable zones (HZs) of stars already made (Y. Fujii et al. 2018; E. W. Schwieterman et al. 2018; C. M. Lisse et al. 2020; D. M. Glaser et al. 2020; M. L. Hill et al. 2023). Traditionally, the HZ is defined as the annular region around a star where liquid water can exist on a planet under sufficient atmospheric pressure.

In modern lexicon, HZs are typically categorized into two broad types (J. F. Kasting et al. 1993; D. R. Underwood et al. 2003). The first is the conservative HZ, which is defined by an inner boundary where the intense radiant energy from the star may induce a runaway greenhouse effect, resulting in the vaporization of surface water. Its outer boundary is determined by the distance from the central star at which a planet's cloud-free CO_2 atmosphere can maintain a surface temperature of 273 K. In contrast, the second type, known as the optimistic habitable zone, encompasses regions receiving radiation levels ranging between those experienced by Mars ∼4 billion years ago and Venus around 1 billion years ago (R. K. Kopparapu et al. 2013, 2014; A. Ware et al. 2022).

In the Galactic context, the conditions favorable for life are also dependent on the spatial and temporal location of star-planet systems within the Milky Way (G. Gonzalez et al. 2001; C. H. Lineweaver et al. 2004). Aspects of galactic habitability include the radiation threat from high-energy events like supernovae (SNe) and gamma-ray bursts (GRBs), the presence of heavy elements that are crucial for the formation of rocky planets, star-forming regions, and the epoch of planet formation in the galaxy (E. Spitoni et al. 2017; R. Spinelli et al. 2021; C. Swastik et al. 2022, 2024; R. Spinelli & G. Ghirlanda 2023).

While the concept of the HZ is vital in the search for habitable worlds, the stellar environment of the planet also plays an important role in determining longevity and the maintenance of habitability. In particular, a planet's habitability can be greatly influenced by the type and distribution of stars surrounding the exoplanet-hosting star. Studies have shown that a high rate of catastrophic events, such as SNe and close stellar encounters in regions of high stellar density, is not conducive to the evolution of complex life forms and the maintenance of habitability over long periods (J. J. Jiménez-Torres et al. 2013; E. Spitoni et al. 2017; R. Spinelli et al. 2021; R. Spinelli & G. Ghirlanda 2023). Important as they are, these theoretical ideas have not been tested against the observed ensemble of extrasolar planets.

The growing number of exoplanet discoveries has enabled researchers to gather robust statistics, warranting further investigation into their stellar environments (M. Narang et al. 2018, 2023; C. Swastik et al. 2021; A. Unni et al. 2022; B. Banerjee et al. 2024). The latest census of confirmed exoplanetary systems and their astrophysical properties are available at various public archives (J. Schneider et al. 2011; R. L. Akeson et al. 2013; E. Han et al. 2014; NASA Exoplanet Science Institute 2020). Out of the 5500+ discovered exoplanets so far, 146 stars are known to host 158 rocky and gaseous planets within their HZs, as

Table 1
Description of the Content of the Table of 84 HZS (with HD 165155 as an Example)

Column Name	Unit	Description	Example Value
Host_Star	⋯	Name of host star	HD 165155
designation	⋯	Gaia DR3 identifier	Gaia DR3 4050...
ra	degrees	Right ascension	271.49
dec	degrees	Declination	−29.92
parallax	mas	Parallax	15.78
pm_ra	mas yr^{-1}	R.A. proper motion	76.89
pm_dec	mas yr^{-1}	Decl. proper motion	−1.57
radial_velocity	km s^{-1}	Radial velocity	15.3
phot_g_mean_mag	*G*-mag	Photometric *G*-band magnitude	9.22
s_teff	K	Surface temperature of host star from NEA	5426
s_logg	log(cm s^{-2})	Surface gravity of host star from NEA	4.49
s_mul	⋯	Number of stars in the system	1
absolute_mag	*G*-mag	Absolute magnitude in *G* band	5.21
S.S.I	⋯	Solar similarity index	0.97
Dispersion_Velocity_log	log(km s^{-1})	Log of dispersion velocity of neighborhood stars	1.690
Dispersion_Velocity_log_std	log(km s^{-1})	Uncertainty in log of dispersion velocity of neighborhood stars	0.003
Object_Den_log	log(pc^{-3})	Log of object density of neighborhood stars	0.388
Object_Den_log_std	log(pc^{-3})	Uncertainty in log of object density of neighborhood stars	0.003
Number	⋯	Number of neighborhood stars	10,235
Number_std	⋯	Uncertainty in number of neighborhood stars	67
D_Teff	K	Dispersion in $T_{\rm eff}$ for neighborhood stars	671
M_Teff	K	Median of $T_{\rm eff}$ for neighborhood stars	3324
D_logg	log(cm s^{-2})	Dispersion in log *g* for neighborhood stars	0.27
M_logg	log(cm s^{-2})	Median of log *g* for neighborhood stars	4.81
D_Ab_Mag	*G*-mag	Dispersion in absolute mag of neighborhood stars	1.05
M_Ab_Mag	*G*-mag	Median of absolute mag of neighborhood stars	15.49
N.S.I	⋯	Neighborhood similarity index	0.527
NSI_std	⋯	Uncertainty in neighborhood similarity index	0.001

Note. "Neighborhood stars" refers to the stars present within the 10 pc environment of their respective HZSs.

(This table is available in its entirety in machine-readable form in the online article.)

documented in the Catalog of Habitable Zone Exoplanets (S. R. Kane & D. M. Gelino 2012; M. L. Hill et al. 2023). Some of these systems are potential targets for detailed atmospheric characterization and the detection of biosignatures in current and future missions (C. C. Stark et al. 2014; G. Tinetti et al. 2018; S. Redfield et al. 2024).

In this work, we focus on the local stellar environment of stars hosting HZ exoplanets. More specifically, we use the Gaia Data Release 3 (DR3) archive to analyze the 10 pc neighborhood (stars within a sphere of 10 pc radius) surrounding the known habitable zone systems (HZSs). This involves extracting sources from the Gaia DR3 archive with measured parallaxes from $\varpi \approx 750$ mas to $\varpi \approx 4.5$ mas, which correspond to the nearest (Proxima Centauri) and the farthest (Kepler-296) HZSs. The rationale for selecting a 10 pc region is based on studies indicating that if a star within this range evolves into a Type Ia/Type Ibc SNe, it would produce X-rays and gamma rays with sufficient fluence (total energy emitted by a SNe per unit area) to significantly disrupt a planet's ozone layer (R. Spinelli & G. Ghirlanda 2023). Additionally, the 10 pc neighborhood of the solar system, well-studied using Gaia DR3 by C. Reylé et al. (2021), provides a valuable reference for exoplanet demographic comparison. We further explore the likelihood of stellar encounters and SNe that could pose a threat to the habitability of these systems. We also compare the 10 pc neighborhood of these HZSs with the 10 pc solar neighborhood sample compiled by C. Reylé et al. (2021) and C. Reylé et al. (2023).

We define the solar similarity index (SSI) as a metric for comparing the properties of the HZ planet-hosting stars with those of the Sun. Similarly, the neighborhood similarity index (NSI) is a metric used to compare the properties and distribution of objects within their respective volumes of 10 pc radius. These indices are then used to determine which habitable systems have the closest resemblance to our solar system and its 10 pc environment. The closer the index is to 1, the more similar it is. The stellar and planetary data (see Table 1) for this study are obtained from the Gaia DR3 and the NASA Exoplanet Archive (NEA; R. L. Akeson et al. 2013; NASA Exoplanet Science Institute 2020; Gaia Collaboration et al. 2023a).

From here on, the paper is organized as follows. In Section 2, we describe our primary sample of HZSs and the construction of their 10 pc neighborhoods. In Section 3, we discuss the influence of the stellar neighborhoods on habitability and present our main results. In Section 4, we address the incompleteness of Gaia data and its implications for our findings. Finally, in Section 5, we summarize and conclude this work.

2. Sample Selection

In this section, we describe the process of our sample selection, which mainly consists of two parts. The first part involves selecting 146 planet-hosting stars from the Habitable Zone Gallery, which constitutes our primary sample of HZSs.[5]

[5] https://hzgallery.org/

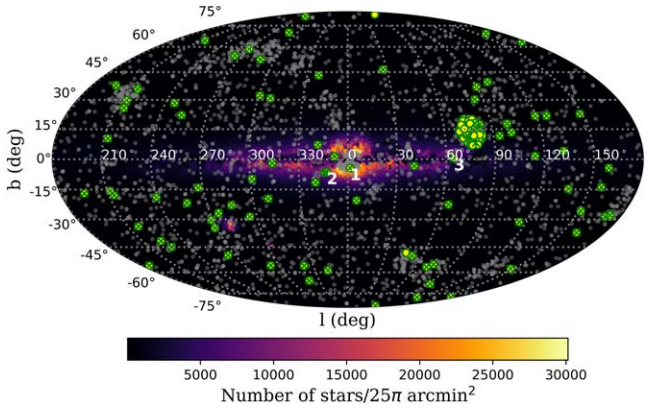

Figure 1. Sky positions of exoplanet-hosting stars projected on a Mollweide map. HZSs are denoted by yellow-green circles, while the remaining population of exoplanets is represented by gray circles. The studied sample of 84 HZSs, located within 220 pc of the Sun, is represented by crossed yellow-green circles. The three high-density HZSs located near the Galactic plane are labeled 1, 2, and 3 in white. The color bar represents the stellar density, i.e., the number of stars having $G \geqslant 15$ within a radius of 5 arcmin.

For the second part, we used the Gaia DR3 catalog to select stars within the 10 pc neighborhood of 144 HZ host stars.[6] The subset of stars in each 10 pc HZ neighborhood was curated from a larger 25 pc data set, as explained in Section 2.2.

2.1. Habitable Zone Gallery

The Habitable Zone Gallery is an online catalog of known exoplanets and their orbital parameters (S. R. Kane & D. M. Gelino 2012; M. L. Hill et al. 2023), constructed using information from larger databases such as the Exoplanet Data Explorer[7] and the NEA.[8] The Gallery demarcates the HZs of each planet-hosting star as defined by R. K. Kopparapu et al. (2013, 2014). It also calculates the fraction of time a planet spends in the HZ, which can vary from 0% to 100% depending on the planet's eccentricity and orbital distance. This catalog is regularly updated and serves as a valuable resource for researchers studying the habitability of exoplanets.

Our primary sample of HZSs, drawn from the Habitable Zone Gallery, comprises 146 systems hosting 158 planets whose orbits fully reside within the optimistic HZ of their host stars. Of these 158 planets, 35 are presumably rocky planets ($\leqslant 2\,R_{\oplus}$), 122 are gaseous planets, and one has an undetermined mass and radius. While the giant planets themselves are inhospitable, they may host rocky exomoons orbiting them under favorable conditions for life (R. Heller 2012; R. Heller & R. Barnes 2013). Additionally, the moons of giant planets located at the outer edge of the HZ could generate sufficient energy through tidal heating (R. Heller & R. Barnes 2013; R. Heller & J. Armstrong 2014; M. L. Hill et al. 2018, 2023). The astrophysical parameters of these systems were obtained from the NASA Exoplanet Archive. Figure 1 shows the all-sky distribution of exoplanet-hosting stars in a Mollweide projection. The nearest HZS to the Sun is Proxima Centauri, located at a distance of 1.3 pc, while the farthest is Kepler-1636, at a distance of 2.2 kpc.

[6] Parallax measurements were not available for two of the systems, Kepler-1652 and Kepler-1410.

[7] http://exoplanets.org/table

[8] https://exoplanetarchive.ipac.caltech.edu/

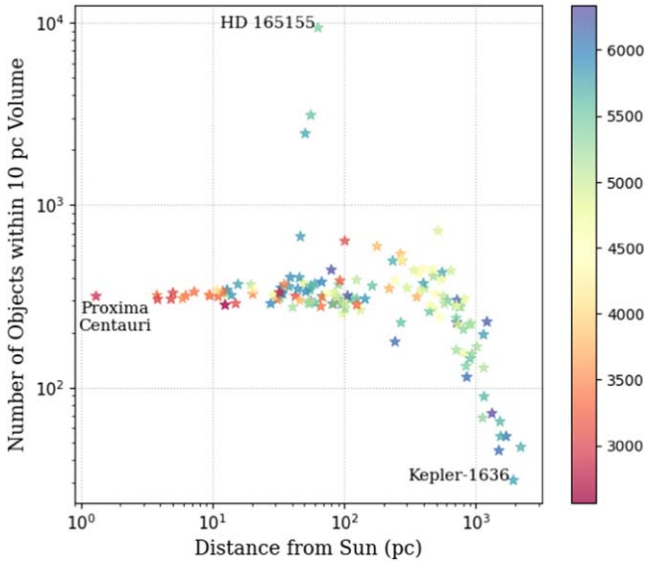

Figure 2. The 10 pc neighborhood star count for 144 HZSs and their distance from the Sun. The color bar represents the effective temperature $T_{\rm eff}$ (in kelvin) of HZ stars.

2.2. Curating the 10 pc Neighborhood

When studying the 10 pc environment of HZSs using Gaia DR3, we have to contend with two major issues:

1. The ambiguity of stars belonging to the 10 pc region due to distance- and magnitude-dependent parallax errors (see Appendix B).
2. The incompleteness of Gaia data, i.e., Gaia's inability to detect sources outside a $21 \lesssim G \lesssim 3$ magnitude range and additional cuts on various astrophysical parameters, impacting its overall data set (C. Reylé et al. 2021; Gaia Collaboration et al. 2023a).

The relative parallax errors in Gaia data can significantly affect distance estimates and introduce ambiguity in defining the 10 pc boundary. This means that a strict 10 pc neighborhood sample returned by a Gaia query (see Figure 2) may include some stars with large parallax errors that could, in reality, be outside the 10 pc sphere, or it may exclude stars that are truly within the 10 pc boundary. Therefore, to address this issue, the 10 pc stellar environment for each HZ system was constructed from a superset of neighboring stars distributed within a sphere of 25 pc radius. For this, we used a simple bootstrapping approach that alleviates the need to define an exact 10 pc boundary and helps constrain the uncertainties of astrophysical parameters of neighborhood stars at the ensemble level, which we later use for quantifying the similarity indices.

Apart from the stated ambiguity in the star count within the 10 pc sample, Figure 2 shows a decline in the number of neighborhood stars around HZSs beyond a distance of ∼300 pc. This selection bias (undercount) arises due to incompleteness of the Gaia data, which is discussed later in Section 4. Figure 3 shows how the relative parallax error of Gaia-detected stars increases with decreasing parallax (i.e., with increasing distance from Sun). Since our goal is to study the 10 pc region around HZ stars, if the distance error were to exceed 10 pc, defining the neighborhood would become arbitrary. For the Gaia-detected stars shown in Figure 3, the relative parallax error exceeds 5% beyond 220 pc ($\varpi \approx 4.5$ mas),

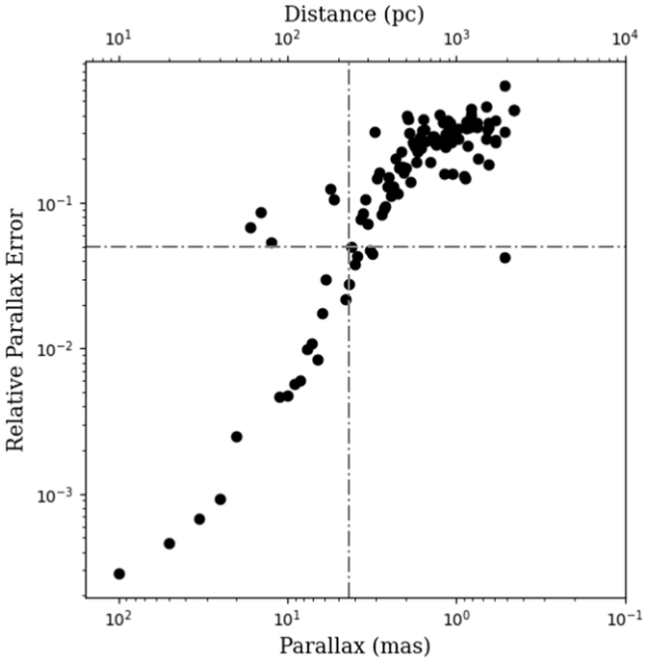

Figure 3. Relative parallax errors of Gaia-detected stars binned at 10 pc intervals as a function of increasing distance from the solar system.

which corresponds to a distance error ∼10 pc. Hence, we only consider 84 HZSs from our primary sample of 146 HZSs, which are within a distance of 220 pc from the Sun. By limiting our sample to 220 pc, we also ensure a nearly complete detection of objects within their 10 pc neighborhood, including the cool dwarfs down to spectral type M6, by Gaia (see Section 4).

To curate a 10 pc sample, we begin by issuing a standard ADQL query on the Gaia DR3 catalog to select stars within 25 pc of a HZS. The query returns all stars around a HZS with distances $\leqslant$25 pc and their astrophysical parameters (see Appendix A). Next, for each HZS, we generate 100,000 random realizations of 10 pc neighborhood stars from this superset by using the bootstrapping method described in Appendix B. The astrophysical parameters and their associated uncertainties are inferred from the sampling distribution of the bootstrap.[9] In Figure 4, we compare the average star count obtained from the bootstrap method and the star count obtained directly from Gaia's 10 pc query for 84 HZSs. Apart from a few outliers, the differences are not significant. However, the bootstrap method provides more reliable estimates of the astrophysical parameters of neighborhood stars.

Finally, the total star count within the 10 pc region surrounding the 84 HZSs is found to be ∼36,000 stars. This data set does not include the brighter stars due to the lower magnitude limit ($G \sim 3$) of Gaia. Finding the bright stars in the vicinity of a HZS is crucial for assessing the threat to habitability from SNe. Therefore, to further complement the 10 pc data set, we separately searched the Hipparcos Catalog (M. A. C. Perryman et al. 1997; F. van Leeuwen 2007) for bright stars.[10] We found 34 bright stars with `hip_mag` <3 belonging to the 10 pc neighborhood of different HZSs. Only two of these 34 bright stars, α-Carinae (around HD 48265) and α-Muscae (around TOI-1227), are massive enough ($\geqslant 8\,M_\odot$) to pose a noteworthy threat to the habitability (see Section 3.2).

3. Results and Discussions

While numerous risks, such as activity-induced stellar winds and superflares from a host star, can compromise a planet's habitability (V. S. Airapetian et al. 2017; C. Garraffo et al. 2017; J. M. Rodríguez-Mozos & A. Moya 2019), here we examine the possibility of any significant impact from stellar encounters and SN explosions in the surrounding stellar environment of a HZS. These events can significantly alter the habitability of planets by displacing them out of their HZ or by disrupting their atmosphere. Studies have shown that the frequency and proximity of such events has a critical role in the habitability of exoplanets within our Galaxy (C. H. Lineweaver et al. 2004; J. J. Jiménez-Torres et al. 2013; E. Spitoni et al. 2017; D. Li et al. 2019, 2020; R. Spinelli et al. 2021; H. Rickman et al. 2022; R. Spinelli & G. Ghirlanda 2023). These factors further determine the long-term viability of habitable conditions on an exoplanet.

3.1. Stellar Encounters

Stellar encounters can impact exoplanetary systems in various ways (J. Horner et al. 2020; N. Davari et al. 2022). A passing star's gravitational influence can perturb distant objects, such as those in the Oort Cloud, pushing them into highly elliptical orbits that may lead to collisions with inner planets. Closer encounters with neighboring stars can directly destabilize planetary orbits, potentially causing planets to migrate inward, outward, or even escape the system entirely. Such disruptions can also alter the eccentricity and inclination of planetary orbits, reducing the time planets spend in the HZ and threatening their habitability (Y.-H. Wang et al. 2020; H. Rickman et al. 2022). In some cases, these perturbations may trigger mechanisms like the Kozai–Lidov effect, leading to oscillations in eccentricity, angular momentum exchange, and changes in orbital inclinations (S. Naoz 2016; M. X. Cai et al. 2017). These orbital shifts may result in variations in stellar insolation flux, which in turn can affect a planet's atmosphere, climate, and potential habitability. Additionally, the destabilization of an outer planet could trigger a cascading effect inward, amplifying instability across planets in the inner orbits. The overall impact of these encounters depends on the mass and proximity of the passing star, as well as the architecture of the planetary system.

J. J. Jiménez-Torres et al. (2013) examined the effect of encounters on habitability in various stellar environments of the Milky Way. They simulated different regions by estimating stellar densities and dispersion velocities, creating a model to approximate the number of close flyby events that can potentially alter the orbital dynamics. They showed that a $1\,M_\odot$ star passing at a distance of 200 au can perturb another stellar system with a radius of 100 au, which has an Oort-like cloud surrounding it. This model is based on the neighborhood's stellar density, dispersion velocity, and evolution time. According to J. J. Jiménez-Torres et al. (2013), the number of encounters, N_e, is given by the following equation:

$$N_e = 4\pi n v T_e R^2, \tag{1}$$

where N_e is the number of encounters, R is the radius of the stellar system ($b = 2R$ is the impact parameter),[11] n is the stellar

[9] See Table 1 for the astrophysical parameters obtained from the statistical inferences of sampling distributions.

[10] Hipparcos Catalog 2007: https://heasarc.gsfc.nasa.gov/W3Browse/all/hipnewcat.html.

[11] The distance of closest approach made by the flyby star to the host star, denoted by b.

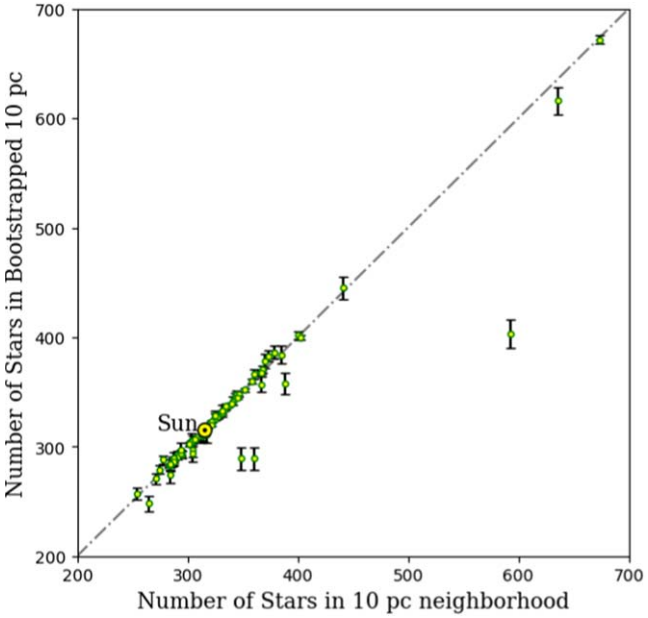

Figure 4. Comparison of number of stars returned by Gaia ADQL query (x-axis) within 10 pc neighborhoods and the 10 pc mean count of stars (y-axis) obtained after 10^5 bootstrap runs on a larger data set of stars within a 25 pc region. The error bars represent $\pm 1\sigma$ uncertainly in the count of stars after bootstrapping. For brevity, the plot is curtailed at 700 star count, excluding three sources with more than 2000 stars.

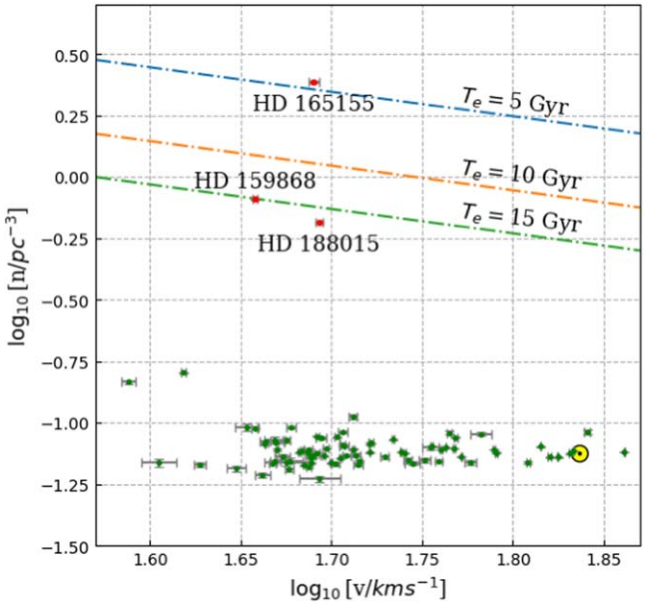

Figure 5. Log–log diagram of stellar density vs. velocity dispersion. Slanted lines indicate the locus of a single encounter ($N_e = 1$) in stellar density–dispersion parameter space for timescales of 5, 10, and 15 Gyr and $b = 150$ au. Three high-stellar-density environments ($> 0.4\,\mathrm{pc}^{-3}$) are shown by red symbols while the remaining low-encounter HZ systems are indicated by green symbols.

density in cubic parsecs, v is the dispersion velocity of the system, and T_e is the evolution time of the system. Although the evidence for Oort-like clouds around exoplanetary systems is still lacking, it is not uncommon to speculate about their existence (J. J. Jiménez-Torres et al. 2013; E. J. Baxter et al. 2018; S. Portegies Zwart et al. 2021). The possibility of planetary bodies residing in Oort-like regions, which can extend up to 100 au from the host star, has also been suggested (S. N. Raymond et al. 2023).

We apply the formalism of Equation (1) to real data (i.e., our HZS sample) and estimate the frequency of gravitational encounters from stars in the 10 pc region of HZSs. We used the proper motions and radial velocity of neighborhood stars to calculate the U, V, and W components using PyAstronomy (S. Czesla et al. 2019; C. Swastik et al. 2023).[12] U denotes the velocity toward the Galactic center, V denotes the velocity in the direction of Galactic rotation, and W denotes the velocity toward the north Galactic pole. Then, we find the dispersion velocity v from $v = \sqrt{\sigma_U^2 + \sigma_V^2 + \sigma_W^2}$, where σ is the dispersion of the respective components.

In these calculations, we used the median mass of neighborhood stars to be $0.3\,M_\odot$, leading to an impact parameter of $b = 150$ au.[13] This is in line with the peak of the stellar mass function (0.3–0.4 $M_\odot$), which is consistent with the general prevalence of low-mass M-type stars in the Milky Way and the solar neighborhood (C. Reylé et al. 2021). The impact parameter $b = 150$ au is determined by calculating the distance at which a neighboring star with a mass of $0.3\,M_\odot$ exerts a gravitational force on the exoplanetary Oort cloud that is equal to the force exerted by a $1\,M_\odot$ star at a distance of $b = 200$ au. Figure 5 shows a log-scaled plot of stellar density versus dispersion velocity for our sample of 84 HZSs. The slanted lines in Figure 5 denote the single-encounter thresholds for timescales of 5, 10, and 15 Gyr. This means that for any HZS to experience at least one encounter within a certain time frame, it must lie on or above the slanted line. Since the stellar density around most HZSs shown in Figure 5 is low ($<0.2\,\mathrm{pc}^{-3}$), they are positioned well below the 15 Gyr line and face a negligible threat to habitability from stellar encounters.

Among the 84 systems, three HZ stars, namely HD 165155, HD 159868, and HD 188015, are residing in a region with an unusually high-stellar-density ($> 0.6\,\mathrm{pc}^{-3}$) environment compared to the Sun and other HZSs. This is not surprising, given that these HZSs are located near the Galactic plane (see Figure 1). However, to rule out erroneous star counts from background contamination and other spurious sources, a further assessment of these three systems is provided in Appendix C.

Notably, HD 165155 is a G8V star with the planet HD 165155 b in its HZ (J. S. Jenkins et al. 2017). This system has the highest stellar density ($n \approx 2.45\,\mathrm{pc}^{-3}$) in our data set, with over $10{,}235 \pm 67$ stars within a 10 pc radius and velocity dispersion $\approx 49\,\mathrm{km\,s}^{-1}$. Given its high-density environment, HD 165155 is expected to undergo at least one stellar encounter within 5 Gyr. In contrast, the other two systems, HD 188015 and HD 159868, have a small likelihood ($N_e < 1$) of experiencing stellar encounters due to their lower stellar density.

Studies on stellar encounters have discussed the evolution of planetary systems in highly dense environments by simulating scenarios with 2000, 8000, and 32,000 stars within a virial radius of 1 pc over a span of 50 Myr (M. X. Cai et al. 2017).[14] They discuss the survival rates of planets in such environments indicating a clear correlation between survival rates and

[12] LSR = (8.5, 13.38, 6.49) (B. Coşkunoğlu et al. 2011).

[13] Masses have been estimated from the updated (2022) table for spectral sequence based on Pecaut & Mamajaek (2013): https://www.pas.rochester.edu/~emamajek/EEM_dwarf_UBVIJHK_colors_Teff.txt.

[14] The radius within which objects exist in a gravitationally bound state.

decreases in stellar density. The work of B. B. Arbab & S. Rahvar (2021) highlighted that the mass and velocity of the flyby stars are crucial in determining the encounter dynamics. Some studies have also discussed the formation of HZ planets in clustered environments and their lifetimes with respect to the stellar mass and the stellar densities of their neighborhoods (M. de Juan Ovelar et al. 2012).

For our HZS sample, the encounter rate was calculated for different n and v. This means the dispersion velocity v was determined for brighter stars, $G \lesssim 15$, for which radial velocity data were available from Gaia DR3 (see Section 4). Since radial velocity data were not available for the fainter stars, the dispersion velocity obtained is only the lower limit. However, due to the shallow slope of the single-encounter lines in Figure 5, underestimation of the dispersion velocity does not affect the encounter rate in any significant way.

3.2. Assessing Threat from SNe Explosions

High-energy particles and radiation arriving from distant regions of space can potentially damage the atmosphere of Earth-like planets or exomoons with an Earth-like atmosphere. Such radiation originates from high-energy transient phenomena, such as GRBs and SNe, which involve a brief period of intense radiation that diminishes over time. Our primary focus is to investigate the effects of SNe on the atmospheres of exoplanets or exomoons, assuming their atmospheres to be Earth-like (B. C. Thomas & A. L. Melott 2006; A. L. Melott & B. C. Thomas 2011; H. M. L. Perkins et al. 2024). The fluence F received by a planet from a high-energy transient event is given by

$$F = \frac{\langle E \rangle}{4\pi r^2}, \tag{2}$$

where $\langle E \rangle$ is the characteristic energy of the event, and r is the distance of the SN from the planet (R. Spinelli et al. 2021; R. Spinelli & G. Ghirlanda 2023). The severity of the ozone depletion would depend on the fluence received by the planet. A fluence $\gtrsim 10\,\mathrm{kJ\,m^{-2}}$ would deplete the ozone layer and make the planet vulnerable to harmful radiation, potentially rendering the planet uninhabitable (B. C. Thomas et al. 2005a, 2005b; A. L. Melott & B. C. Thomas 2011; J. E. Horvath & D. Galante 2012; R. Spinelli & G. Ghirlanda 2023). In our study, we primarily focus on SNe Ibc and SNe II since their occurrence is relatively higher than other sources of X-ray and gamma-ray radiation such as GRBs and SNe Ia (W. Li et al. 2011; R. Spinelli & G. Ghirlanda 2023).

It is well established that a Type Ib,c or a Type II SNe requires a progenitor star with a mass exceeding $8\,M_\odot$. While SNe Ia are formed from binary accreting systems involving a degenerate star, SNe Ibc and SNe II are formed from core collapse (R. Spinelli & G. Ghirlanda 2023). The typical characteristic energy of an SNe ranges from a minimum of 10^{33} kJ (SNe II) to a maximum of 10^{37} kJ (SNe I; R. Spinelli et al. 2021; R. Spinelli & G. Ghirlanda 2023). Therefore, we focus on identifying stars with mass $\geqslant 8\,M_\odot$ within 10 pc of each HZ system, as outlined by R. Spinelli & G. Ghirlanda (2023). Gaia's Final Luminosity Age Mass Estimator (FLAME) package provides an estimate of stellar mass (O. L. Creevey et al. 2023; M. Fouesneau et al. 2023; Gaia Collaboration et al. 2023b), but it is not available for all the stars in our sample. We use the mass–luminosity relationship

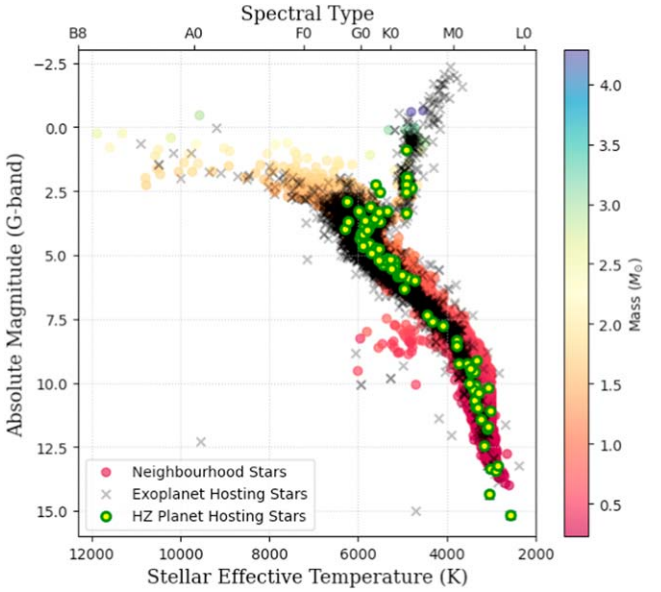

Figure 6. HR diagram of all Gaia-detected stars in a 10 pc region of 84 HZSs and the known exoplanet-hosting stars. The neighborhood stars are color-coded according to their estimated mass.

described by J. Wang & Z. Zhong (2018) in Equation (3) to estimate masses for stars in our data set that lack FLAME-derived mass estimates:

$$\frac{M}{M_\odot} = \left(\frac{L}{L_\odot}\right)^{\frac{1}{4}} \left(\frac{1}{3}\right)^{(T_{\rm eff}/T_\odot)^{\frac{1}{3}}-1}. \tag{3}$$

Here, L is the luminosity, M is the mass, and $T_{\rm eff}$ is the surface temperature of the star. We used Pogson's formula in Equation (3) to calculate luminosity from absolute magnitudes (N. Pogson 1856; I. Ibrahim et al. 2018) for stars without FLAME luminosity. In our analysis of the Gaia DR3 data set, we do not find any star with a $M \geqslant 6\,M_\odot$ surrounding HZS.

Figure 6 shows a Hertzsprung–Russell (HR) diagram of our full Gaia data set of neighborhood stars. To convert from effective temperature to spectral type, we referred to the updated spectral sequence based on M. J. Pecaut & E. E. Mamajek (2013).[15] The HR diagram shows that the neighborhood stars in our sample range from type L0 to B8. Since stars brighter than $G \leqslant 3$ are absent in the Gaia catalog, we searched the Hipparcos Catalog (M. A. C. Perryman et al. 1997; F. van Leeuwen 2007) and found two HZSs (TOI-1227 and HD 48265) with high-mass stars ($M > 8\ M_\odot$), namely α-Muscae and α-Carinae, respectively, within their 10 pc vicinity.[16] These stars are potential SNe progenitors. We consider the evolution of these high-mass stars into SNe Ibc as the worst-case scenario from the viewpoint of habitability of the central HZS. The maximum characteristic energy, $\langle E \rangle$, that a SNe Ibc would produce is $\sim 10^{37}$ kJ.

The variation of fluence received from SNe explosions as a function of distance and characteristic energy released is illustrated in Figure 7. In the figure we depict two high-mass stars that are located at a distance $\lesssim 10$ pc from HZSs TOI-1227

[15] Updated (2022) table for spectral sequence based on Pecaut & Mamajaek (2013): https://www.pas.rochester.edu/~emamajek/EEM_dwarf_UBVIJHK_colors_Teff.txt.

[16] Hipparcos Catalog 2007: https://heasarc.gsfc.nasa.gov/W3Browse/all/hipnewcat.html.

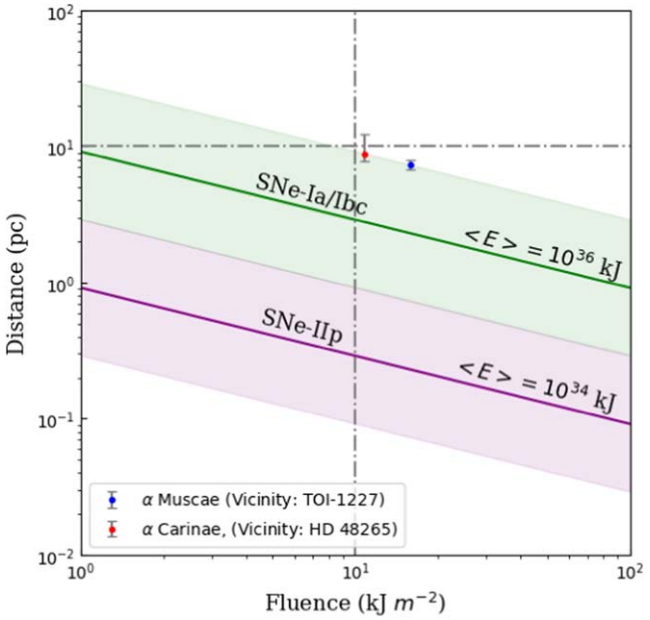

Figure 7. Fluence received from SNe explosions as a function of distance. The purple and green bands depict the range of energy released from different SNe. The shaded region to the right of the vertical line receives a fluence in excess of 10 kJ m^{-2}, which is considered harmful to habitability. The locations of two high-mass stars ($M > 8\,M_{\odot}$), which are potential progenitors of SNe, are also shown for comparison.

and HD 48265. A resulting stellar explosion (SNe Ibc) releasing a maximum energy $\langle E \rangle = 10^{37}$ kJ would produce a lethal fluence $\geqslant$10 kJ m^{-2} of X-rays/gamma rays (R. Spinelli & G. Ghirlanda 2023) within a 10 pc sphere. The planets in these two systems, namely TOI-1227 b (A. W. Mann et al. 2022) and HD 48265 b (D. Minniti et al. 2009), are gaseous. Although these planets themselves cannot have habitable conditions, they might host exomoons that could have Earth-like atmospheres susceptible to these effects. For an Earth-like atmosphere this could deplete ∼68% of the ozone layer (B. C. Thomas & A. L. Melott 2006; R. Spinelli et al. 2021).

Note that GRBs can emit immense energy, affecting planets as far as ∼1 kpc away (R. Spinelli et al. 2021; R. Spinelli & G. Ghirlanda 2023). However, due to the unpredictability and rarity of GRB events, we do not consider them within the scope of the present work. Similarly, predicting whether a main-sequence white dwarf binary will undergo a Type Ia SNe is challenging, as it depends on factors like their proximity and the orbital dynamics of a compact binary system. In contrast, the likelihood of Type Ibc and Type II SNe is higher in stars with masses $\geqslant 8\,M_{\odot}$. In a worst-case scenario, if a high-mass star is stripped of its hydrogen envelope, it will evolve into a SNe Ib. If both hydrogen and helium are depleted, it will become a SNe Ic. However, it is rare for a high-mass star to evolve into these categories by losing sufficient hydrogen from its outer layers. In most cases, a high-mass star undergoes core collapse, producing less energetic SNe II, which indicates their impact is less damaging beyond 5 pc (A. L. Melott et al. 2017). None of our HZSs have high-mass stars within a 5 pc region. Recent studies also suggest that a SNe explosion occurring even at distances up to 20 pc could be lethal to a planet's habitability (B. C. Thomas & A. M. Yelland 2023).

3.3. Similarity Indices

The discovery of numerous extrasolar planets has revealed a diverse array of stellar and planetary characteristics, making systematic comparisons crucial for evaluating habitability and assessing the potential for life beyond our solar system. For example, Sun-like stars are more likely to host stable habitable environments for their planetary systems due to the moderate nature of their stellar activity (A. Loeb et al. 2016; M. Lingam & A. Loeb 2017a, 2017b; J. Haqq-Misra et al. 2018). Additionally, the overall stellar environment of the solar system (e.g., the location in the galaxy, neighborhood stellar spectral types, density, and dispersion velocity) appears conducive to the long-term maintenance of habitable conditions (J. J. Jiménez-Torres et al. 2013; E. Spitoni et al. 2017; R. Spinelli et al. 2021; R. Spinelli & G. Ghirlanda 2023) and may serve as a valuable reference for comparison (C. Reylé et al. 2021, 2023). Furthermore, since the Sun has played a crucial role in the evolution and maintenance of life on Earth, assessing the similarity of other planet-hosting stars to the Sun is of paramount importance.

The similarity index is a numerical metric used to quantify the likeness or resemblance between objects or systems sharing specific properties. This concept has been previously applied to assess the resemblance of known extrasolar planets to Earth by comparing their mass, radius, and surface temperature (S.-H. Cha 2007; D. Schulze-Makuch et al. 2011). In this study, we employ the concept of a similarity index to assess the resemblance and dissimilarity between 84 habitable systems and their stellar environments. Specifically, we utilize two distinct similarity indices:

1. *Solar similarity index (SSI).* This index allows for a comparison of the properties of our solar system with those of corresponding HZSs.
2. *Neighborhood similarity index (NSI).* This index facilitates a comparison of the properties of stars in the 10 pc volume around the solar system and the neighborhood stars of the HZS.

We define each similarity index as

$$SSI,\, NSI = 1 - \sqrt{\frac{1}{n}\sum_{i=1}^{n}\left(\frac{P_i - P_{i\odot}}{P_i + P_{i\odot}}\right)^2}, \tag{4}$$

where P_i refers to the value of the ith stellar parameter chosen for comparison, while $P_{i\odot}$ is the corresponding value for the Sun or the solar system, and n denotes the number of parameters considered.

To calculate the SSI using Equation (4), we selected four parameters, namely stellar multiplicity, effective temperature, surface gravity, and absolute magnitude. Likewise, to calculate the NSI for each HZS, we chose eight parameters for the ensemble of stars within the 10 pc region. These parameters include the dispersion velocity of stars (σ_v), the median and standard deviation of temperature ($\langle T_{\rm eff} \rangle$ and $\sigma_{T_{\rm eff}}$), the median and standard deviation of absolute magnitude ($\langle {\rm mag} \rangle$ and $\sigma_{\rm mag}$), the median and standard deviation of $\log g$ ($\langle \log g \rangle$ and $\sigma_{\log g}$), and finally the neighborhood star count.

The SSI was calculated directly from Equation (4) for each HZ star, using stellar parameters taken from NEA. For the NSI of a stellar environment, we used the bootstrap method to generate 100,000 neighborhood configurations. We then

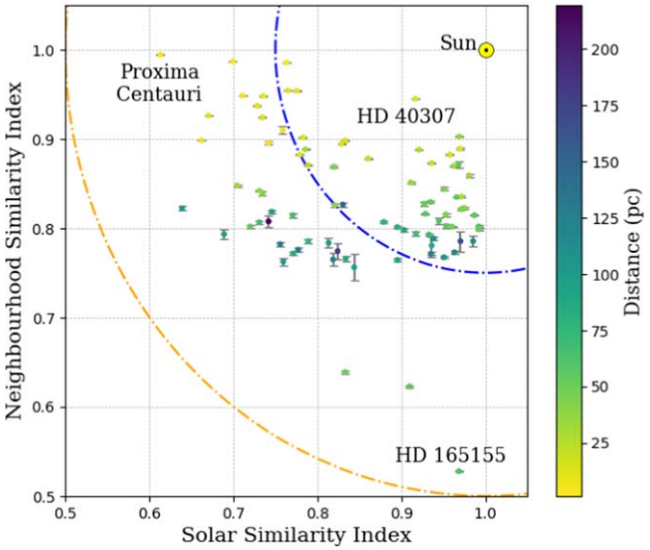

Figure 8. Similarity-index-based comparison of HZSs with the solar system. The color bar represents the distance of the HZSs from the Sun in parsec. The blue and orange semicircles centered on the Sun correspond to 0.75 and 0.50 similarity in the NSI–SSI plane.

derived the NSI value from the median of this sampling distribution and its associated uncertainties from the standard deviation (see Appendix B).

The plot of NSI versus SSI in Figure 8 shows a comparison of different HZSs with the solar system and stars in their respective 10 pc neighborhood. The HZSs within the blue circle represent a similarity greater than 0.75, while those with a similarity of more than 0.50 fall within the orange circle. Overall, we note that the NSI is >0.75 for most HZSs, implying a high degree of similarity between the stellar environment of the Sun and the HZ stars. Also, the HZSs nearer to the solar neighborhood tend to have a higher NSI due to the presence of a similar population of stars. The differences however tend to grow with an increase in distance, as is evident from the vertical color gradient seen in Figure 8. On the other hand, the SSI values have a larger spread, primarily due to the different spectral types of stars in the HZ sample.

More specifically, in Figure 8 we note that HD 40307, a K2.5V dwarf star with $T_{\rm eff} \approx 5000$ K, located 13 pc from the Sun and hosting a 7.1 $M_{\oplus}$ HZ planet, HD 40307 g (M. Mayor et al. 2009; M. Tuomi et al. 2013; R. Brasser et al. 2014), has the highest overall similarity index among the 84 HZSs. This system has an NSI of 0.94 and a SSI of 0.92, and five planets discovered in its system. The NSI of Proxima Centauri is highest because its 10 pc volume significantly overlaps with the stars in the 10 pc neighborhood of the Sun. However, Proxima Centauri is a red dwarf star ($T_{\rm eff} \approx 3000$ K) which is cooler and smaller than the Sun, and it is also part of a multiple star system. These differences contribute to its low SSI as seen in Figure 8. Conversely, HD 165155 is a G-type HZ star with a high SSI but low NSI. This is largely due to its densely populated surrounding, containing nearly 10,000 stars, in stark contrast to the 315 stars in the 10 pc solar neighborhood.

Exoplanet demographic studies have shown that the solar system is somewhat uncommon in terms of both its planetary properties such as mass, radius, orbital period, eccentricity, and distribution in the system, as well as the stellar properties of the Sun (J. N. Winn & D. C. Fabrycky 2015; R. G. Martin & M. Livio 2015; W. Zhu & S. Dong 2021). Many studies have tried to find stars that closely resemble the Sun, particularly in terms of fundamental stellar parameters, activity, rotation rate, and elemental abundances (I. Ramírez et al. 2009; J. Datson et al. 2015; D. Mahdi et al. 2016). Our current treatment of the SSI is somewhat simplistic. It is not intended to capture all the nuances and subtleties required to establish or refute the uniqueness of the Sun or the solar system among the known exoplanetary systems. Settling this question—one way or another—would require more data and improved characterization of host stars, which future ground-based and space missions will hopefully provide.

4. Completeness of Gaia Data

Instrument sensitivities limit the detection of stars, as well as the measurement of stellar properties and the quantities derived from them (M. Fouesneau et al. 2023). Therefore, a given instrument is capable of detecting and characterizing only a certain fraction of the true number of objects (the ground truth); this fraction is called its completeness. The completeness of detections and the measurement/estimation of stellar astrophysical parameters (e.g., radial velocity, $T_{\rm eff}$, etc.) in Gaia DR3 depends on various factors, which include source crowding in the field of observation and the "scanning law" (number of visits Gaia made to that patch of the sky; T. Cantat-Gaudin et al. 2023). This affects the accuracy of our results outlined in the previous section. In the following subsections, we discuss the completeness of our sample and its impact on threat assessment from stellar encounters and the interpretation of similarity indices.

4.1. Detection Completeness

Stellar encounters heavily depend on the density of the stellar neighborhood; the number of stars is one of the parameters required to calculate the NSI. Gaia is able to detect objects with apparent magnitudes ranging from $G \approx 3$ to $G \approx 21$ (D. W. Evans et al. 2018). Based on the simplified assumption that the solar neighborhood is a good representative of the demographics of stars within ~250 pc, we can conclude that bright stars constitute a small fraction of the population, whereas low-mass M dwarfs and ultracool dwarfs constitute the majority of the population (C. Reylé et al. 2021). Figure 9 shows the demographics of the Gaia-detected 10 pc sample of neighborhood stars as a function of spectral type and distance from the Sun. At closer distances, the detection of most stars is nearly complete. The detection sensitivity begins to decline as the distance increases; however, this decline is faster for late-spectral-type stars than for early-spectral-type stars. Although T5 dwarfs have been detected in our sample up to 20 pc and the faintest source detected at 240 pc is an M8 dwarf, this does not guarantee a complete detection of similar sources. A single detection may be attributed to Gaia's large number of visits to the corresponding patch of sky or to a relatively darker background (T. Cantat-Gaudin et al. 2023). In reality, there might be many more M dwarfs and brown dwarfs in a given region than the few detections suggest.

The completeness of Gaia DR3 was derived by T. Cantat-Gaudin et al. (2023) by comparing detections of Gaia DR3 against that of DECaPS (A. K. Saydjari et al. 2023).[17] Gaia has a complex scanning law, and its performance varies significantly between sparse and densely populated regions of the sky. Therefore, the

[17] The Dark Energy Camera Plane Survey (DECaPS) was a ground-based deep survey of the southern Galactic plane.

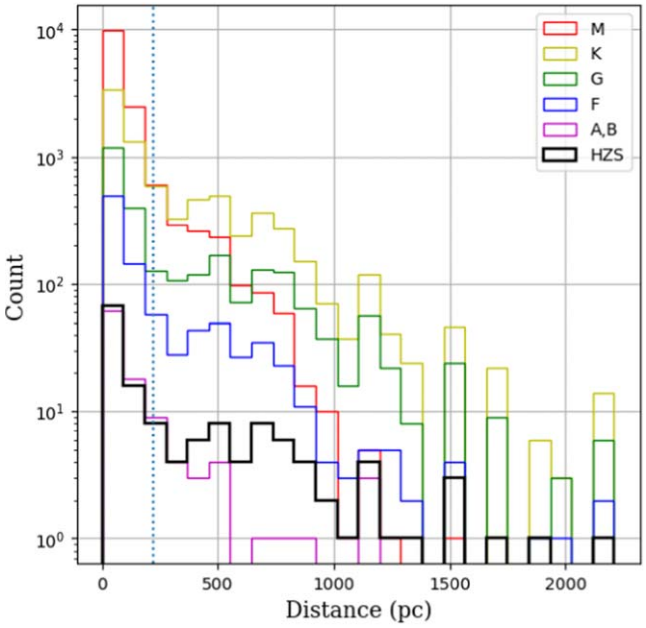

Figure 9. Distribution of Gaia-detected neighborhood stars and HZSs. The source count is a function of spectral type and distance from the Sun. Eighty-four out of 146 HZSs studied in this work lie within a distance of 220 pc (marked by a vertical dotted line) from the Sun.

number of useful visits, and hence the total integration time of Gaia, is not the same throughout the sky. These factors result in anisotropy of the median magnitude of stars detected by Gaia in a particular patch of sky. T. Cantat-Gaudin et al. (2023) use the median magnitude of stars, M, to account for the anisotropic selection biases of Gaia while empirically modeling its completeness.[18] Figure 10 shows the sky distribution of the faintest magnitude of stars in the Galactic reference system, to which Gaia is at least 95% complete. This map was generated using the `gaiaunlimited` package developed by T. Cantat-Gaudin et al. (2023). The overlaid green points show the positions of 84 HZSs that we analyze. This figure provides a qualitative description of the sky distribution of the apparent magnitude to which a particular HZS's neighborhood (fixed M) is 95% complete.

DECaPS is a deep survey with a small footprint (6.5% sky coverage). Further, it is not complete to the faintest brown dwarfs, and therefore does not represent the ground truth. Although it can provide a good reference to estimate Gaia's overall completeness, this method is not entirely reliable for computing the true counts for neighborhoods of individual HZSs. We have therefore used a selection function (see Section 2.3 of T. Cantat-Gaudin et al. 2023) to estimate the completeness as a function of the spectral type of stars in HZS neighborhoods.[19]

For a particular spectral type, (i.e., certain absolute G magnitude), the apparent magnitude increases with distance. For every HZ system, (different M, varying Galactic cooordinates) we compute the completeness using the selection function developed by T. Cantat-Gaudin et al. (2023). Figure 11 shows how the completeness of neighborhood stars of different spectral types varies with distance. Notably, the detection of all stars up to the M spectral type is nearly complete for HZSs within ∼80 pc from the Sun. The location of the farthest exoplanetary system analyzed in our HZ sample, Kepler-296, is marked by a vertical line drawn at 220 pc in Figure 11. We note that the stellar neighborhood of Kepler-296 is almost complete for M5.5V-type stars, ∼70% complete for M6V-type stars, whereas ultracool dwarfs (later than M6V-type stars) have a significantly lower likelihood of being detected.

4.2. Completeness of Astrophysical Parameters

The three main instruments on board Gaia include an astrometric instrument for precise stellar position and parallax measurements, a broadband photometer for measuring stellar brightness, and a radial velocity spectrometer to determine the velocity of stars along the line of sight. The radial velocity spectra (RVS) are also used to estimate parameters like $T_{\rm eff}$ and $\log g$. The photometric instrument provides the color information along with apparent magnitude, $T_{\rm eff}$, and $\log g$. Recio-Blanco et al. 2023; O. L. Creevey et al. (2023) and M. Fouesneau et al. (2023) provide a detailed discussion on Gaia's estimates and the accuracy of astrophysical parameters. Generally, the stellar parameters obtained using RVS are more accurate than those obtained using photometry. Gaia uses three methods to estimate $T_{\rm eff}$ and $\log g$: a generalized stellar parametrizer (GSP), an extended stellar parametrizer (ESP), and a multiple star classifier (MSC). We obtained the stellar parameters of neighborhood stars from Gaia by following the priority order (from highest to lowest) GSP-Spec, GSP-Phot, ESP-HS, ESP-UCD, MSC-1, and MSC-2.[20] GSP-Spec mainly operates on stars with $G \lesssim 15$, GSP-Phot on $G \lesssim 19$, MSC on $G \lesssim 18.25$, and ESP-HS and ESP-UCD operate on hot stars and ultracool dwarfs, respectively (M. Fouesneau et al. 2023; Recio-Blanco et al. 2023; O. L. Creevey et al. 2023).

Figure 12 illustrates the completeness of various astrophysical parameters obtained from Gaia as a function of the apparent G magnitude of stars. Notably, the data for most parameters are complete up to $G \approx 15$. Beyond that the completeness differs for each parameter. For example, the complete radial velocity data are only available for stars with $G \lesssim 15$, whereas $T_{\rm eff}$ and $\log g$ data are available for the majority of stars detected up to $G \lesssim 17.5$. These magnitude limits are further described in M. Fouesneau et al. (2023).

The foregoing discussions demonstrate that our 10 pc neighborhood data set is incomplete both in terms of source detections and the availability of astrophysical parameters from Gaia. This incompleteness directly impacts the results presented in Section 3. For example, a fraction of low-mass faint stars at larger distances would remain undetected, leading to an underestimation of stellar density in the 10 pc region. Consequently, the estimated stellar encounter rates represent a lower limit of the actual values. Likewise, the completeness of astrophysical parameters is biased toward the brighter stars. This indicates that the median values of stellar parameters such as $T_{\rm eff}$ and $\log g$ derived from their respective bootstrap distributions are overestimated, while the neighborhood star count n and absolute magnitude M_G are underestimated. This introduces a completeness-dependent bias in the estimation of the NSI. Although this bias in NSI is minimized by restricting

[18] Median magnitude of stars with useful visits (the Gaia parameter, `astrometric_matched_transits`) $\gtrsim$10, referred to in T. Cantat-Gaudin et al. (2023) as M_{10}. We refer to it as M here for simplicity.

[19] Empirical model for Gaia completeness: a sigmoid function with M and apparent magnitude as its parameters.

[20] "Spec": spectroscopy; "Phot": photometry, "HS": hot stars; "UCD": ultracool dwarfs.

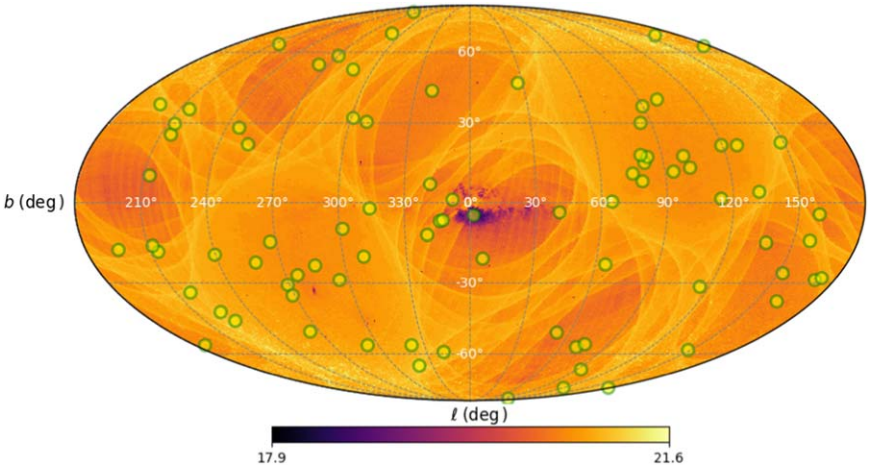

Figure 10. The 95% completeness map of the Gaia-scanned region in Galactic coordinates (l and b), generated using the `gaiaunlimited` package (T. Cantat-Gaudin et al. 2023). The color scale indicates the faintest G magnitude at which the 95% completeness threshold is achieved. Our sample of 84 HZSs (green circles) has been overlaid on the map to visually depict the completeness of their respective neighborhoods.

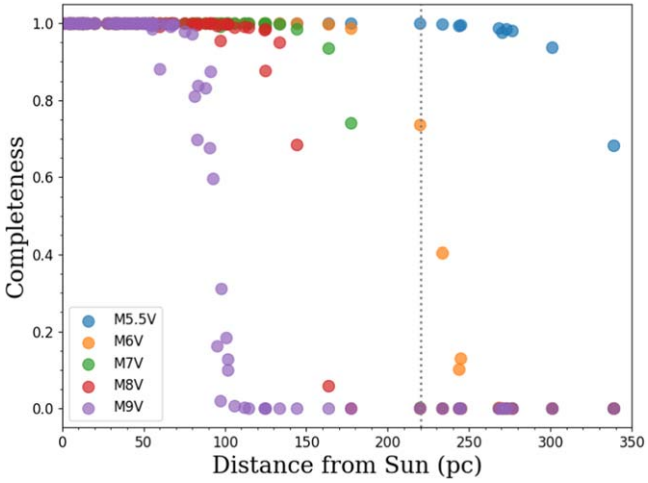

Figure 11. Gaia completeness of neighborhood stars as a function of distance. Different colors represent different spectral types. Each point corresponds to a HZ system.

our analysis to the 84 HZSs closest to the Sun, it is not entirely eliminated.

5. Summary and Conclusion

The quest to find habitable planets is a key area of study in exoplanet research. More than 150 confirmed detections of planets in the HZs of various stars have been made. The origin and stability of habitable conditions depend on the star-planet system's location in the Milky Way and are influenced by factors such as high-energy radiation from SNe, the presence of heavy elements, and the epoch of planet formation. High rates of catastrophic events in dense stellar regions can hinder the long-term evolution and survival of habitability. For a planet to remain habitable, it must retain its atmosphere, be shielded from harmful radiation, and maintain a stable orbit within its HZ without being perturbed by other gravitational influences. The astrophysical impacts of stellar environment is a "low-probability, high-consequence" scenario for the continuation of the habitability of exoplanets. Even a single disruptive event of this kind, though less likely, could significantly impact the planet's habitability.

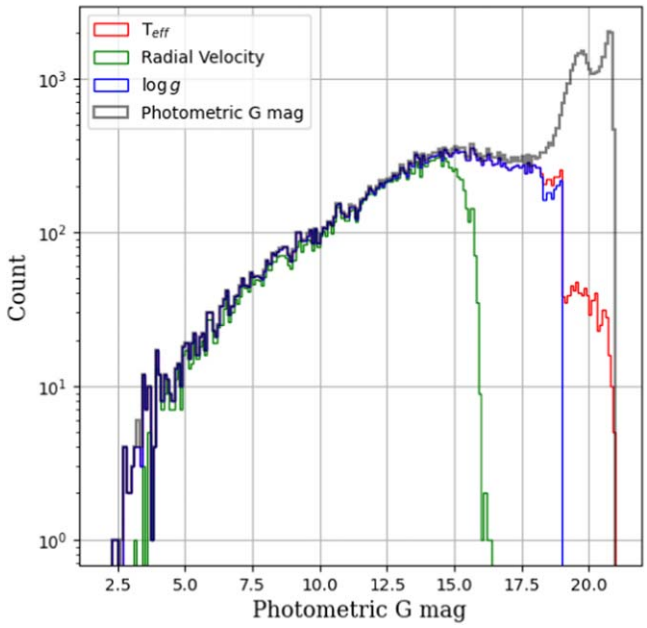

Figure 12. Distribution of photometric mean G magnitude for objects with available $T_{\rm eff}$, $\log g$, and radial velocity in Gaia.

In this study, we focused on the 10 pc neighborhood around known HZ systems to investigate the potential threats to their habitability from nearby stellar encounters and SNe. To accomplish these goals, we analyzed the astrometric, photometric, and spectroscopic data of these environments using Gaia DR3 and Hipparcos. We used a bootstrap approach to construct the 10 pc neighborhoods of HZ systems, discussed the influence of stellar environments on habitability, and highlighted the limitations due to the incompleteness of Gaia data. We also developed two metrics, the SSI and the NSI, to compare the properties of the 10 pc environments of HZ systems with the 10 pc environment of our solar system.

Out of the 84 HZSs studied, three systems have a stellar density of $\geqslant 0.4\,{\rm pc}^{-3}$. Among these, only one system, HD 165155, has an encounter rate of $\geqslant 1$ in a 5 Gyr period, increasing the likelihood of perturbation of planetary orbits during the star's main-sequence evolution. We found a high-mass star ($>8\,M_{\odot}$) within the 10 pc neighborhoods of each of

two HZSs, namely TOI-1227 and HD 48265. These high-mass stars are potential progenitors for SN explosions. Energy released from these stellar explosions can deposit a high fluence of harmful radiation on distant planets (or their exomoons), stripping off their ozone layer and rendering them uninhabitable. Upon comparing the 10 pc solar and stellar neighborhoods, we find that the stellar environments of the majority of HZSs exhibit a high degree of similarity (NSI > 0.75) to the solar neighborhood. Due to the diverse spectral types of HZ planet-hosting stars, when we compare them with the Sun we get a wide range of SSI values.

Finally, we discussed the possible limitations of this study due to the incompleteness of Gaia data. We find that our sample of different HZSs' neighborhood stars is complete to early M-type stars. Incompleteness starts to plague our sample for ultracool dwarfs (later than M6V) at ∼220 pc. We also show that instruments on board Gaia are biased to brighter stars; Gaia DR3 completely catalogs all astrophysical parameters only until $G \lesssim 15$. Therefore, by volume-limiting our sample to 84 HZSs within 220 pc, we partially mitigated the uncertainties injected into our analysis due to Gaia's completeness bias. Because of this incompleteness, the computed stellar encounter probabilities are lower limits, and comparison between solar system and the exo-HZSs is not accurate. However, our analysis provides a preliminary basis for characterizing the stellar environments of exoplanetary systems and warrants the need for more complete surveys.

From the perspective of habitability, investigating the local stellar environments of planet-hosting stars is an interesting and challenging problem that will benefit from more complete and accurate data. The forthcoming Gaia Data Release 4 promises enhanced completeness and precision in estimating the astrophysical parameters of stars, which will improve our capability to fully characterize the 10 pc neighborhood of HZ stars. Additionally, future deep-sky surveys will further enhance our ability to investigate the stellar neighborhoods of planet-hosting stars at greater distances.

Acknowledgments

This work has made use of data from the European Space Agency (ESA) mission Gaia (https://www.cosmos.esa.int/gaia), processed by the Gaia Data Processing and Analysis Consortium (DPAC, https://www.cosmos.esa.int/web/gaia/dpac/consortium). Funding for the DPAC has been provided by national institutions, in particular the institutions participating in the Gaia Multilateral Agreement. This research has made use of data obtained through the High Energy Astrophysics Science Archive Research Center Online Service, provided by the NASA/Goddard Space Flight Center. This work has also referred to the NASA Exoplanet Archive and the Habitable Zone Catalog (S. R. Kane & D. M. Gelino 2012). This research has made use of the Exoplanet Orbit Database and the Exoplanet Data Explorer at exoplanets.org. T.P. would also like to thank the Indian Institute of Astrophysics, for providing the necessary support during this work. Finally, the authors sincerely thank the anonymous reviewer for their valuable comments and suggestions, which have helped us improve the quality of this manuscript.

Software: NumPy (C. R. Harris et al. 2020), PyAstronomy (S. Czesla et al. 2019; https://github.com/sczesla/PyAstronomy), Astroquery (A. Ginsburg et al. 2019), Matplotlib (J. D. Hunter 2007).

Appendix A
Function to Obtain 25 pc Samples

```
from astroquery.gaia import Gaia as ga

def nearby25(par,dec,ra):
query = "SELECT *
FROM gaiadr3.gaia_source as g
JOIN gaiadr3.astrophysical_parameters AS ap ON g.
  source_id = ap.source_id
WHERE SQRT(POWER((1000/g.parallax)*COS(RADIANS(g.
  dec))*COS(RADIANS(g.ra))
- 1000/"+str(par)+"*COS(RADIANS("+str(dec)+"))*COS
  (RADIANS("+str(ra)+")),2) +
POWER((1000/g.parallax)*COS(RADIANS(g.dec))*SIN
  (RADIANS(g.ra))
- 1000/"+str(par)+"*COS(RADIANS("+str(dec)+"))*SIN
  (RADIANS("+str(ra)+")),2) +
POWER((1000/g.parallax)*SIN(RADIANS(g.dec))
- 1000/"+str(par)+"*SIN(RADIANS("+str(dec)
  +")),2)) < = 25 AND g.parallax > 0"

r = ga.launch_job_async(query)
res = r.get_results()

return res
```

The above code defines a function, `nearby25`, that queries the Gaia DR3 archive to find stars within a 25 pc radius of a HZS based on its `parallax` (in milliarcseconds), `ra`, and `dec`. The Gaia parallax (ϖ) is converted to the radial distance from the Sun by simple inversion $r = 1/\varpi$. The query also joins data from two Gaia DR3 tables, `gaia_source` and `astrophysical_parameters`, based on a common `source_id`.

The code converts the spherical polar coordinates (r, θ, ϕ) to Cartesian coordinates (x, y, z). It makes the following assumptions to do so:

1. The x-axis extends from the origin O through the vernal equinox along the equatorial plane. This axis aligns with 0° R.A.
2. The y-axis, orthogonal to the x-axis within the equatorial plane, points toward 90° R.A.
3. The z-axis is perpendicular to the equatorial plane.

To be consistent with spherical geometry, we define, $\phi =$ R.A. (angle made with x-axis) and $\theta = 90$–decl. (angle made with z-axis). These spherical polar coordinates (r, θ, ϕ) are then converted to Cartesian coordinates (x, y, z) via the following transformation:

$$\begin{aligned} x &= r \sin\theta \cos\phi \\ y &= r \sin\theta \sin\phi \\ z &= r \cos\theta. \end{aligned} \tag{A1}$$

The distance between the HZ star (x, y, z) and a neighboring star (x', y', z') in a 10 pc region is calculated using $d = \sqrt{(x-x')^2 + (y-y')^2 + (z-z')^2}$. In summary, for each HZ system the three input parameters parallax, decl., and R.A. define its spatial location. Gaia DR3 is queried for the spatial locations of stars detected within 25 pc of the HZS using the `nearby25` function, which is defined above. This 25 pc volume of stars around a HZ system is then used to construct the 10 pc neighborhood of stars using the bootstrapping algorithm as explained in Appendix B.

Appendix B
Constructing the 10 pc Stellar Neighborhood Using the Bootstrap Method

Bootstrapping is a resampling technique employed in statistics to estimate the sampling distribution of a quantity by creating multiple simulated data sets from an original sample. This process involves randomly selecting data points from the original data set with replacement, constructing new samples of the same size as the original (A. C. Davison et al. 2003; K. M. Ramachandran & C. P. Tsokos 2021). To construct the 10 pc neighborhood of each HZS, we applied the bootstrap method to Gaia-detected stars within their 25 pc volume. To visualize how the algorithm resamples in order to construct new configurations of neighborhoods in each iteration, we consider a hypothetical data set of n neighborhood stars (original 25 pc data from Gaia) with known parallaxes and parallax errors as shown in the upper-left panel of Figure 13. The blue and red circles represent the 10 pc and the 25 pc neighborhood boundary, respectively. This algorithm is shown as a flowchart in Figure 14. We assume the measured parallax of each star j follows a Gaussian distribution $\mathcal{N}_j(\varpi_j, \sigma_{\varpi j})$, where ϖ_j is the mean parallax and $\sigma_{\varpi j}$ is the standard deviation. In bootstrap, we randomly draw n stars from the original sample $\{\mathcal{N}_j(\varpi_j, \sigma_{\varpi j}\}_{j=1}^{n}$ and select those for which $r = 1/\varpi \leqslant 10$ pc. Applying this cutoff causes some stars originally outside the 10 pc boundary to move inside, while some stars initially within the boundary move beyond the 10 pc limit. This creates a new sample of a 10 pc neighborhood. Three random realizations of the bootstrap process are illustrated in the top-right panel and the bottom row of Figure 13. The likelihood of a star crossing the 10 pc boundary strongly depends on the original parallax ϖ and the associated parallax error σ_{ϖ}. This means that, for each random draw, stars near the 10 pc boundary in the original sample are more likely to move in and out of the 10 pc region compared to stars significantly closer to or farther from the center. For each iteration we count the

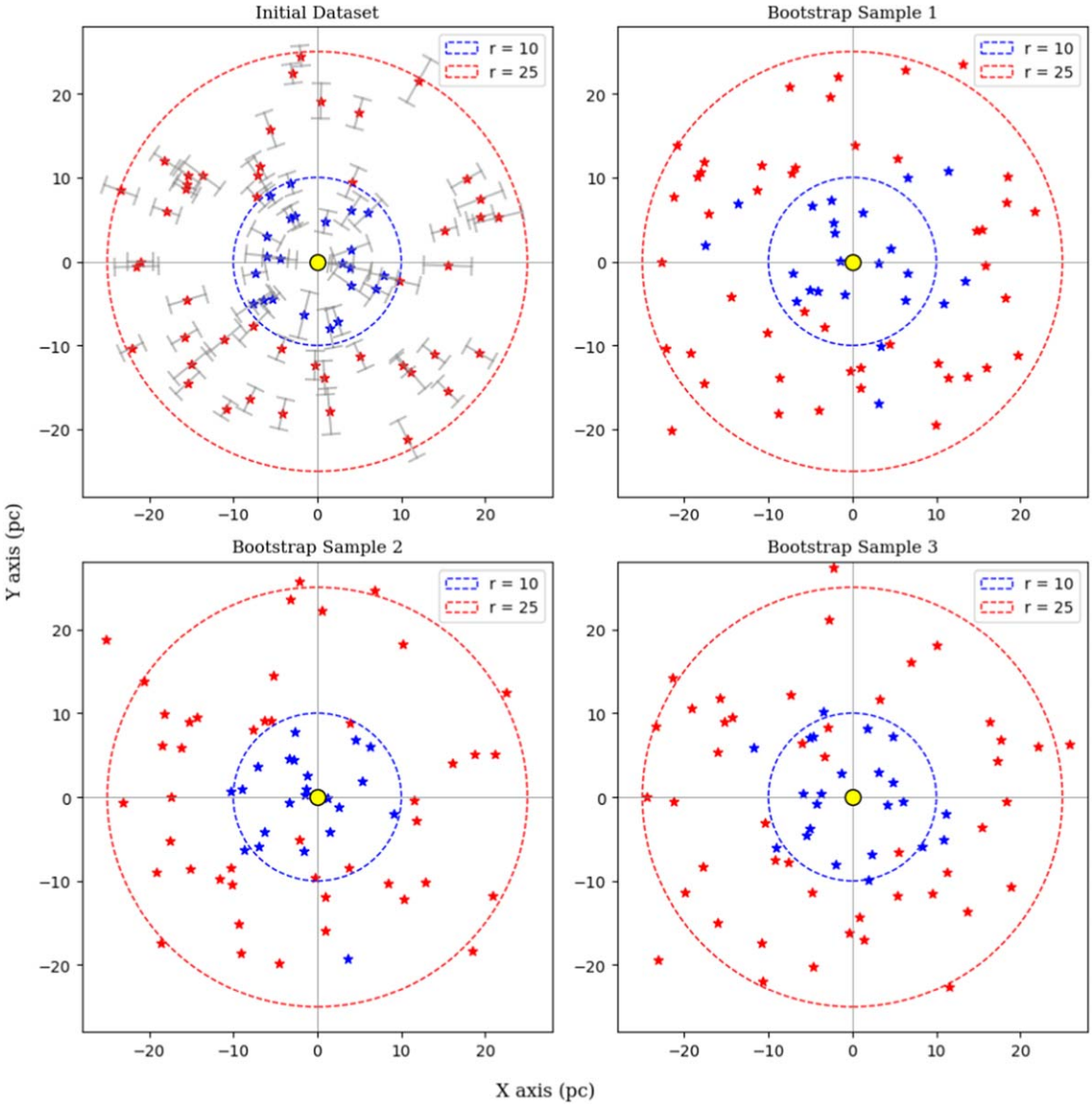

Figure 13. Top left: the initial data set of stars with measured parallaxes (ϖ) and $\pm 1\sigma_{\varpi}$ errors projected on a 2D plane. The blue symbols are stars residing within a 10 pc radius denoted by the blue circle, and red symbols are stars in a 25 pc radius denoted by the red circle. Top right and bottom row: three randomly drawn samples from the original distribution showing some of the stars crossing the 10 pc boundary.

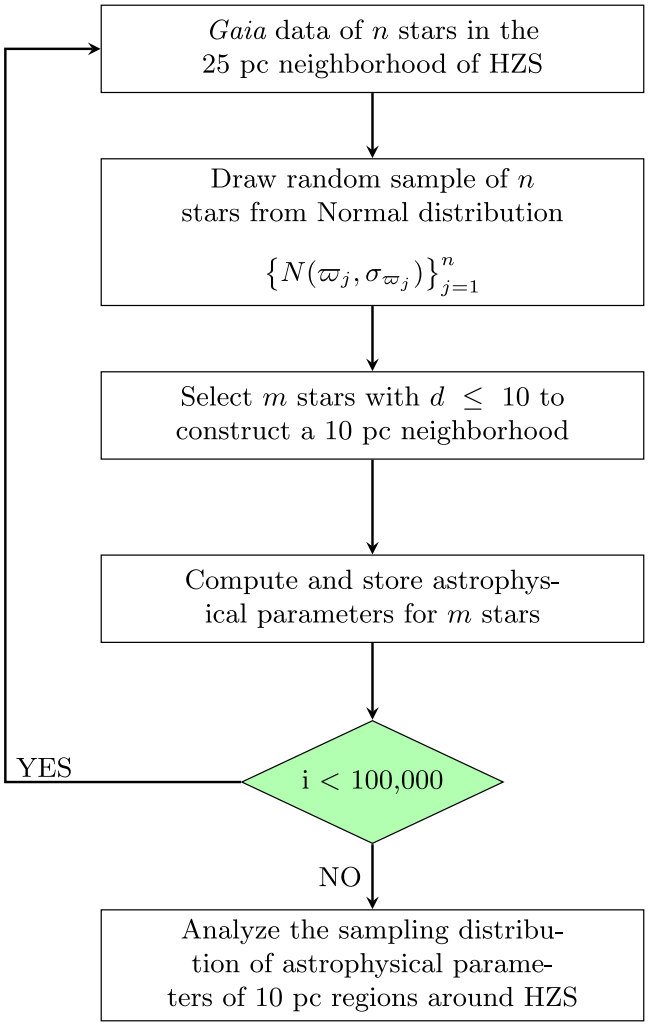

Figure 14. Schematic of the bootstrapping algorithm used for constructing a 10 pc neighborhood of HZ planet-hosting stars.

number of stars in the 10 pc region and also keep track of their astrophysical parameters. After 10^5 bootstrap runs we get a sampling distribution of each parameter. The median and standard deviation of these distributions are taken as parameters of interest (e.g., dispersion velocity, number density, etc.).

This is a quantitative way to statistically estimate the uncertainties introduced by parallax errors in constructing the 10 pc neighborhood of HZSs. The bootstrapping algorithm described above provides us with the sampling distribution of neighborhood astrophysical parameters used for our analysis. For example, the results for a system, HD 165155, are shown in Figure 15. For more than 20,000 realizations, the neighborhood is found to have 10,200 stars, while on none of the occasions do we find 10,500 or more stars. The median and standard deviation have been obtained from these sampling distributions for star count and astrophysical parameters such as $\langle \log g \rangle$, $\langle T_{\rm eff} \rangle$, and $\langle$AbsoluteMagnitude$\rangle$. We conclude from this analysis that HD 165155 has $10{,}235 \pm 67$ stars with a median $T_{\rm eff}$ of 3324 ± 28 K, median log g of 4.81 ± 0.01, and median absolute magnitude of 15.490 ± 0.003. The astrophysical parameters of all 84 HZSs and their 10 pc neighborhood stars, estimated using bootstrap, are provided in a machine-readable table (Table 1).

Appendix C
10 pc Neighborhoods with High Densities

We have studied the 10 pc neighborhood of 84 HZSs and identified three systems—HD 165155, HD 159868, and HD 188015—that stand out due to their unusually high star densities. HD 165155, located ∼63 pc away, with ∼10,000 stars in its 10 pc vicinity, has a local neighborhood star density 30 times larger than the Sun and the majority of other HZSs studied. HD 159868 and HD 188015, while showing lower densities, still contain ∼3400 and ∼2700 stars, respectively, which is about 10 times greater than the local density of the Sun's neighborhood. Given their positions at or near the Galactic plane, these high-density regions might initially seem unrealistic, raising the possibility of inclusion of spurious sources or contamination of the sample by background stars. Such artifacts can also arise from diffraction spikes of bright stars, source confusion, faults in telescope behavior, or transiting solar system objects (F. Torra et al. 2021). We carefully analyzed these high-density regions to address the serious concern of sample contamination.

We first confirmed that all three high-density HZSs are indeed located near the Galactic plane (see Figure 1), where the background star density is particularly high. In addition to HD 165155, HD 159868, and HD 188015, there are five other HZSs located in the foreground of the high-density region of the Galactic plane, though their 10 pc volume does not differ significantly from that of the Sun. This dissimilarity implies that the neighborhood data compiled from Gaia DR3 is highly accurate and reliable, even for HZSs located near the Galactic plane.

We also find that the distance between HD 165155 and HD 159868 is 16.5 pc, indicating that both systems are embedded in a similar stellar environment. In contrast, HD 188015 is about 60 pc away from these systems and roughly 50 pc from the Sun, which happens to be a relatively less dense environment.

J. Rybizki et al. (2022), developed a classifier for Gaia Early Data Release 3 sources to identify astrometric solutions as either `good` or `bad`. They set the `parallax_over_error` threshold >4.5 for high signal-to-noise ratio regimes. In our data ∼99% of the sources within the 10 pc neighborhood of these high-density regions fall in that regime. Moreover, their analysis indicates that at a threshold of `parallax_over_error` >10, the number of `bad` sources is <10%. This serves as a strong constraint for good astrometric sources.

As an additional and independent test, we also employed Monte Carlo simulations to estimate the statistical likelihood of observing high-stellar-density regions within the 100 pc solar neighborhood. To this end, a raw sample of ∼570,000 stars was compiled by selecting all stellar sources with a Gaia-measured parallax of ⩾10 mas. From this 100 pc sample, we randomly selected points in R.A. [0,360], decl. [−90,90], and parallax [11.11,1000] mas, and for each point we counted the number of stars within its 10 pc neighborhood. This process was repeated one million times. We found that the probability of obtaining >10,000 stars in 10 pc volume around random locations is 0.14% and that of obtaining >2000 is 1.7%. These results suggest that, while the neighborhoods of the three HZSs in question seem rare, the occurrence of dense regions of stars within 100 pc of the Sun is not entirely improbable.

Finally, we plot the 25 pc neighborhood star count for the 84 HZSs in Figure 16. Similar to the 10 pc region, the 25 pc star

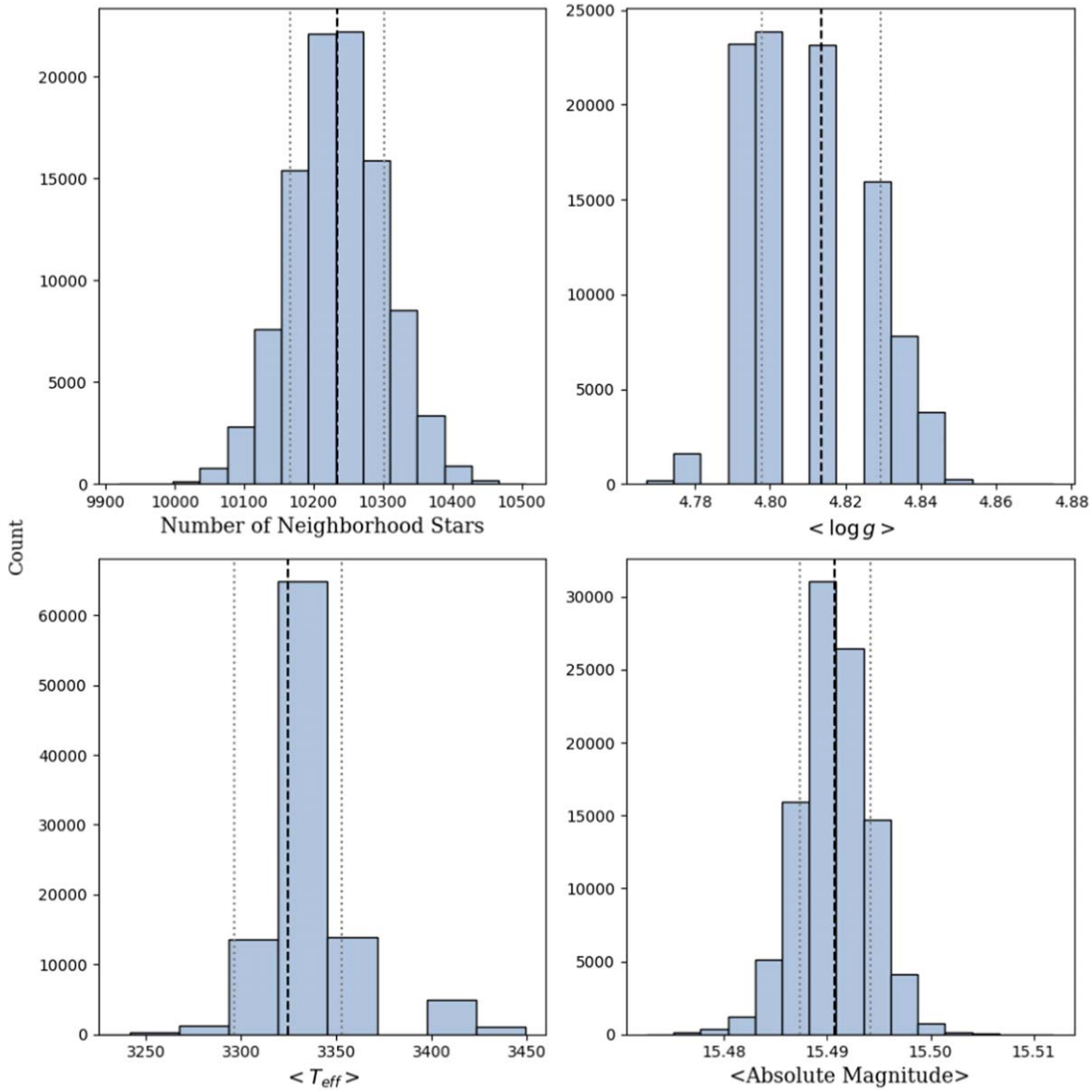

Figure 15. Bootstrapped sampling distributions of neighborhood star count (top left) and astrophysical parameters: $\langle \log g \rangle$ (top right), $\langle T_{\rm eff} \rangle$ (bottom left), and $\langle$AbsoluteMagnitude$\rangle$ (bottom right) of the 10 pc environment of HD 165155. Gray dotted lines represent the standard deviation and black dashed lines represent the median.

count around HD 165155 remains highest (∼77,000), followed by ∼45,000 stars around HD 159868. However, the 15-fold increase in volume resulted in less than an eightfold increase in star count, indicating a notable density drop in going from the 10 pc to the 25 pc region. We would not expect such a drop if the background stars near the Galactic plane were contaminating the neighborhood sample.

Figure 17 represents the distribution of the `parallax_over_error` for sources within the 25 pc radius of the three HZSs that have the highest population within their 10 pc radius and three HZSs that have a lower population (<1000) in their 10 pc neighborhood. This plot indicates that most environments have a majority of sources with high signal-to-noise ratio (`parallax_over_error` $\gtrsim 10$) and hence have good astrometric solutions (J. Rybizki et al. 2022). The sharp decline on the left slope also suggests the presence of a smaller number of high-parallax-error sources. A value $\geqslant$10 indicates that the parallax error does not result in a distance error $\geqslant$10 pc for any source within 100 pc. The closer the object, the lesser is the error in distance. In conclusion, although our neighborhood sample may not be entirely free from spurious sources, the robust astrometric solutions from Gaia, combined with our bootstrap approach, provide a reliable method for studying the neighborhood demographics of HZSs.

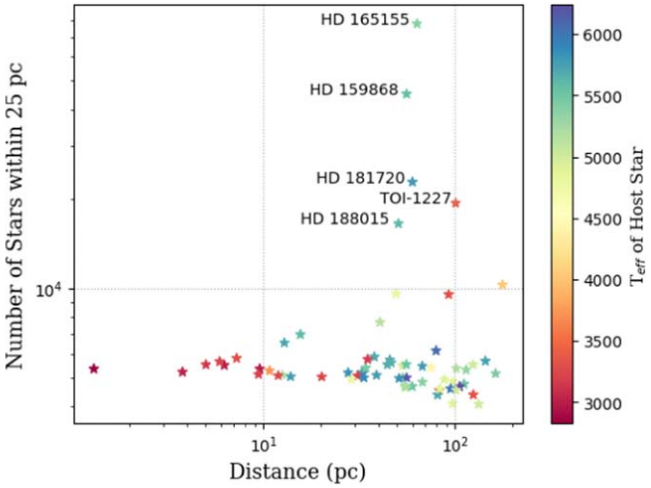

Figure 16. The 25 pc neighborhood star count for 84 HZSs and their distance from the Sun. The color bar represents the effective temperature $T_{\rm eff}$ (in kelvin) of HZ stars. The names of the five HZSs with the highest star count are also labeled.

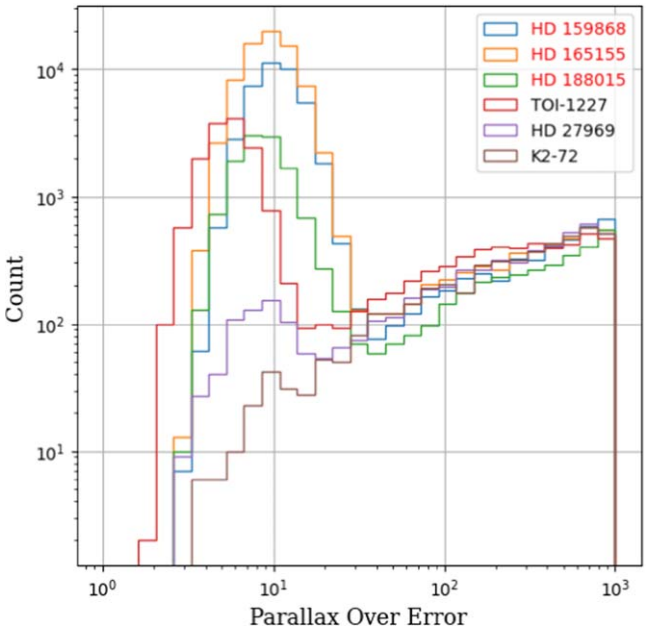

Figure 17. Distribution of `parallax_over_error` for stars in a 25 pc neighborhood around six HZSs. The names of the three HZSs with the highest star count in their 10 pc regions are indicated in the legend with red.

ORCID iDs

Ravinder K. Banyal https://orcid.org/0000-0003-0799-969X
C. Swastik https://orcid.org/0000-0003-1371-8890
Ayanabha De https://orcid.org/0000-0001-8845-184X

References

Airapetian, V. S., Glocer, A., Khazanov, G. V., et al. 2017, ApJL, 836, L3
Akeson, R. L., Chen, X., Ciardi, D., et al. 2013, PASP, 125, 989
Arbab, B. B., & Rahvar, S. 2021, IJMPD, 30, 2150063
Banerjee, B., Narang, M., Manoj, P., et al. 2024, AJ, 168, 7
Baxter, E. J., Blake, C. H., & Jain, B. 2018, AJ, 156, 243
Brasser, R., Ida, S., & Kokubo, E. 2014, MNRAS, 440, 3685
Cai, M. X., Kouwenhoven, M. B. N., Portegies Zwart, S. F., & Spurzem, R. 2017, MNRAS, 470, 4337
Cantat-Gaudin, T., Fouesneau, M., Rix, H.-W., et al. 2023, A&A, 669, A55
Cha, S.-H. 2007, City, 1, 1
Coşkunoğlu, B., Ak, S., Bilir, S., et al. 2011, MNRAS, 412, 1237
Creevey, O. L., Sordo, R., Pailler, F., et al. 2023, A&A, 674, A26
Czesla, S., Schröter, S., Schneider, C. P., et al., 2019 PyA: Python Astronomy-related Packages, Astrophysics Source Code Library, ascl:1906.010
Datson, J., Flynn, C., & Portinari, L. 2015, A&A, 574, A124
Davari, N., Capuzzo-Dolcetta, R., & Spurzem, R. 2022, MNRAS, 513, 90
Davison, A. C., Hinkley, D. V., & Young, G. A. 2003, StaSc, 18, 141
de Juan Ovelar, M., Kruijssen, J. M. D., Bressert, E., et al. 2012, A&A, 546, L1
Evans, D. W., Riello, M., De Angeli, F., et al. 2018, A&A, 616, A4
Fouesneau, M., Frémat, Y., Andrae, R., et al. 2023, A&A, 674, A28
Fujii, Y., Angerhausen, D., Deitrick, R., et al. 2018, AsBio, 18, 739
Gaia Collaboration, Creevey, O. L., Sarro, L. M., et al. 2023b, A&A, 674, A39
Gaia Collaboration, Vallenari, A., Brown, A. G. A., et al. 2023a, A&A, 674, A1
Garraffo, C., Drake, J. J., Cohen, O., Alvarado-Gómez, J. D., & Moschou, S. P. 2017, ApJL, 843, L33
Ginsburg, A., Sipőcz, B. M., Brasseur, C. E., et al. 2019, AJ, 157, 98
Glaser, D. M., Hartnett, H. E., Desch, S. J., et al. 2020, ApJ, 893, 163
Gonzalez, G., Brownlee, D., & Ward, P. 2001, Icar, 152, 185
Han, E., Wang, S. X., Wright, J. T., et al. 2014, PASP, 126, 827
Haqq-Misra, J., Kopparapu, R. K., & Wolf, E. T. 2018, IJAsB, 17, 77
Harris, C. R., Millman, K. J., van der Walt, S. J., et al. 2020, Natur, 585, 357
Heller, R. 2012, A&A, 545, L8
Heller, R., & Armstrong, J. 2014, AsBio, 14, 50
Heller, R., & Barnes, R. 2013, AsBio, 13, 18
Hill, M. L., Bott, K., Dalba, P. A., et al. 2023, AJ, 165, 34
Hill, M. L., Kane, S. R., Seperuelo Duarte, E., et al. 2018, ApJ, 860, 67
Horner, J., Kane, S. R., Marshall, J. P., et al. 2020, PASP, 132, 102001
Horvath, J. E., & Galante, D. 2012, IJAsB, 11, 279
Hunter, J. D. 2007, CSE, 9, 90
Ibrahim, I., Malasan, H. L., Kunjaya, C., et al. 2018, RAA, 18, 041
Jenkins, J. S., Jones, H. R. A., Tuomi, M., et al. 2017, MNRAS, 466, 443
Jiménez-Torres, J. J., Pichardo, B., Lake, G., & Segura, A. 2013, AsBio, 13, 491
Kane, S. R., & Gelino, D. M. 2012, PASP, 124, 323
Kasting, J. F., Whitmire, D. P., & Reynolds, R. T. 1993, Icar, 101, 108
Kopparapu, R. K., Ramirez, R., Kasting, J. F., et al. 2013, ApJ, 765, 131
Kopparapu, R. K., Ramirez, R. M., SchottelKotte, J., et al. 2014, ApJ, 787, L29
Li, D., Mustill, A. J., & Davies, M. B. 2019, MNRAS, 488, 1366
Li, D., Mustill, A. J., & Davies, M. B. 2020, MNRAS, 496, 1149
Li, W., Leaman, J., Chornock, R., et al. 2011, MNRAS, 412, 1441
Lineweaver, C. H., Fenner, Y., & Gibson, B. K. 2004, Sci, 303, 59
Lingam, M., & Loeb, A. 2017a, ApJ, 848, 41
Lingam, M., & Loeb, A. 2017b, ApJL, 846, L21
Lisse, C. M., Desch, S. J., Unterborn, C. T., et al. 2020, ApJL, 898, L17
Loeb, A., Batista, R. A., & Sloan, D. 2016, JCAP, 2016, 040
Mahdi, D., Soubiran, C., Blanco-Cuaresma, S., & Chemin, L. 2016, A&A, 587, A131
Mann, A. W., Wood, M. L., Schmidt, S. P., et al. 2022, AJ, 163, 156
Martin, R. G., & Livio, M. 2015, ApJ, 810, 105
Mayor, M., Udry, S., Lovis, C., et al. 2009, A&A, 493, 639
Melott, A. L., & Thomas, B. C. 2011, AsBio, 11, 343
Melott, A. L., Thomas, B. C., Kachelrieß, M., Semikoz, D. V., & Overholt, A. C. 2017, ApJ, 840, 105
Minniti, D., Butler, R. P., López-Morales, M., et al. 2009, ApJ, 693, 1424
Naoz, S. 2016, ARA&A, 54, 441
Narang, M., Manoj, P., Furlan, E., et al. 2018, AJ, 156, 221
Narang, M., Oza, A. V., Hakim, K., et al. 2023, AJ, 165, 1
NASA Exoplanet Archive 2020, Planetary Systems, IPAC, doi:10.26133/NEA12
Pecaut, M. J., & Mamajek, E. E. 2013, ApJS, 208, 9
Perkins, H. M. L., Ellis, J., Fields, B. D., et al. 2024, ApJ, 961, 170
Perryman, M. A. C., Lindegren, L., Kovalevsky, J., et al. 1997, A&A, 323, L49
Pogson, N. 1856, MNRAS, 17, 12
Portegies Zwart, S., Torres, S., Cai, M. X., & Brown, A. G. A. 2021, A&A, 652, A144
Ramachandran, K. M., & Tsokos, C. P. 2021, in Mathematical Statistics with Applications in R, ed. K. M. Ramachandran & C. P. Tsokos (3rd ed.; New York: Academic Press), 531
Ramírez, I., Meléndez, J., & Asplund, M. 2009, A&A, 508, L17
Raymond, S. N., Izidoro, A., & Kaib, N. A. 2023, MNRAS, 524, L72
Recio-Blanco, A., de Laverny, P., Palicio, P. A., et al. 2023, A&A, 674, A29
Redfield, S., Batalha, N., Benneke, B., et al. 2024, arXiv:2404.02932
Reylé, C., Jardine, K., Fouqué, P., et al. 2021, A&A, 650, A201
Reylé, C., Jardine, K., Fouqué, P., et al. 2023, in The 21st Cambridge Workshop on Cool Stars, Stellar Systems, and the Sun, Cambridge

Workshop on Cool Stars, Stellar Systems, and the Sun (Cambridge: Cambridge Univ. Press), 218
Rickman, H., Wajer, P., Przyłuski, R., et al. 2022, MNRAS, 520, 637
Rodríguez-Mozos, J. M., & Moya, A. 2019, A&A, 630, A52
Rybizki, J., Green, G. M., Rix, H.-W., et al. 2022, MNRAS, 510, 2597
Saydjari, A. K., Schlafly, E. F., Lang, D., et al. 2023, ApJS, 264, 28
Schneider, J., Dedieu, C., Le Sidaner, P., Savalle, R., & Zolotukhin, I. 2011, A&A, 532, A79
Schulze-Makuch, D., Méndez, A., Fairén, A. G., et al. 2011, AsBio, 11, 1041
Schwieterman, E. W., Kiang, N. Y., Parenteau, M. N., et al. 2018, AsBio, 18, 663
Spinelli, R., & Ghirlanda, G. 2023, Univ, 9, 60
Spinelli, R., Ghirlanda, G., Haardt, F., Ghisellini, G., & Scuderi, G. 2021, A&A, 647, A41
Spitoni, E., Gioannini, L., & Matteucci, F. 2017, A&A, 605, A38
Stark, C. C., Roberge, A., Mandell, A., & Robinson, T. D. 2014, ApJ, 795, 122
Swastik, C., Banyal, R. K., Narang, M., Unni, A., & Sivarani, T. 2024, AJ, 167, 270
Swastik, C., Banyal, R. K., Narang, M., et al. 2021, AJ, 161, 114
Swastik, C., Banyal, R. K., Narang, M., et al. 2022, AJ, 164, 60
Swastik, C., Banyal, R. K., Narang, M., et al. 2023, AJ, 166, 91
Thomas, B. C., Jackman, C. H., Melott, A. L., et al. 2005a, ApJ, 622, L153
Thomas, B. C., & Melott, A. L. 2006, NJPh, 8, 120
Thomas, B. C., Melott, A. L., Jackman, C. H., et al. 2005b, ApJ, 634, 509
Thomas, B. C., & Yelland, A. M. 2023, ApJ, 950, 41
Tinetti, G., Drossart, P., Eccleston, P., et al. 2018, ExA, 46, 135
Torra, F., Castañeda, J., Fabricius, C., et al. 2021, A&A, 649, A10
Tuomi, M., Anglada-Escudé, G., Gerlach, E., et al. 2013, A&A, 549, A48
Underwood, D. R., Jones, B. W., & Sleep, P. N. 2003, IJAsB, 2, 289
Unni, A., Narang, M., Sivarani, T., et al. 2022, AJ, 164, 181
van Leeuwen, F. 2007, A&A, 474, 653
Wang, J., & Zhong, Z. 2018, A&A, 619, L1
Wang, Y.-H., Perna, R., & Leigh, N. W. C. 2020, MNRAS, 496, 1453
Ware, A., Young, P., Truitt, A., & Spacek, A. 2022, ApJ, 929, 143
Winn, J. N., & Fabrycky, D. C. 2015, ARA&A, 53, 409
Zhu, W., & Dong, S. 2021, ARA&A, 59, 291